### Title
High figure-of-merit p-type transparent conductor, Cu alloyed ZnS via radio frequency magnetron sputtering




### Journal
Journal of Physics D, 50(50)

### ISSN
0022-3727



### Authors
Maurya, Sandeep Kumar
Liu, Ya
Xu, Xiaojie
et al.



### Publication Date
2017-12-20

### DOI
10.1088/1361-6463/aa95b3

Peer reviewed

# High figure-of-merit *p*-type transparent conductor, Cu alloyed ZnS *via* radio frequency magnetron sputtering

**Sandeep Kumar Maurya[1,2], Ya Liu[2,3], Chandan Das[1], Xiaojie Xu[2,4], Rachel Woods-Robinson[2], Joel W. Ager III[2,5], K.R. Balasubramaniam[1]**

[1]Department of Energy Science and Engineering, Indian Institute of Technology Bombay, Mumbai 400076, India.

[2]Materials Sciences Division, Lawrence Berkeley National Laboratory, Berkeley, CA USA.

[3]International Research Center for Renewable Energy, State Key Laboratory of Multiphase Flow in Power Engineering, Xi'an Jiaotong University, Xi'an, Shaanxi, 710049, P. R. China

[4]Department of Materials Science, Fudan University, Shanghai 200438, P. R. China.

[5]Department of Materials Science and Engineering, University of California Berkeley, Berkeley, CA USA.

E-mail: bala.ramanathan@iitb.ac.in

**Abstract.** *p*-type transparent conducting Cu alloyed ZnS thin films from $Cu_xZn_{1-x}S$ targets (x = 0.1, 0.2, 0.3, 0.4, and 0.5) were deposited on glass substrates *via* radio frequency (RF) sputtering. XRD and TEM–SAED analysis show that all the films have sphalerite ZnS as the majority crystalline phase. In addition, films with 30% and 40% Cu show the presence of increasing amounts of crystalline $Cu_2S$ phase. Conductivity values $\geq$ 400 S $cm^{-1}$ were obtained for the films having 30% and 40% Cu, with the maximum conductivity of 752 S $cm^{-1}$ obtained for the film with 40% Cu. Temperature dependent electrical transport measurements indicate metallic as well as degenerate hole conductivity in the deposited films. The reflection-corrected transmittance of this Cu alloyed ZnS (40% Cu) film was determined to be $\geq$ 75% at 550 nm. The transparent

conductor figure of merit ($\Phi_{TC}$) of the Cu alloyed ZnS (40% Cu), calculated with the average value of transmittance between 1.5 to 2.5 eV, was $\approx 276$ $\mu$S.

*Keywords*: Transparent conductor, hole conductor, RF sputtering, figure of merit

Submitted to: *J. Phys. D: Appl. Phys.*

## 1. Introduction

Wide band gap oxide materials such as fluorine doped tin oxide (FTO), Aluminum doped zinc oxide (AZO) and tin doped indium oxide (ITO) are very well known $n$-type transparent conductors [1, 2]. These $n$-type transparent materials are widely used in optoelectronic devices such as LEDs and solar photovoltaics (PV) [3, 4, 5]. However, the counterpart $p$-type transparent conductors are comparatively less investigated [6]. The first $p$-type transparent conductor, $CuAlO_2$ crystallizing in the delafossite structure, was reported in 1997 by Kawazoe *et al.* possessing a hole conductivity $\approx$ 0.1 S cm$^{-1}$ at room temperature [7]. Since then, there have been a number of experimental reports of $p$-type transparent conductors, but in general most of the reported $p$-type transparent conductors show very low conductivity compared to the $n$-type transparent conductors [6, 8, 9]. The doped and undoped Cu-based compounds such as K doped $SrCu_2O_2$ [10], $CuMO_2$ (M = Ga, In, Sc, Y) [11, 12, 13, 14], LaCuOQ (where Q = S, Se) [15, 16], constitute the typical materials that have been studied. These materials show good transmittance in the visible light range but the presence of localized oxygen $2p$ orbitals at the valence band maximum (VBM) pose a fundamental problem. Majority of the metal oxides have VBM effective mass greater than 1 $m_e$ (mass of electron), which gives rise to low hole mobility [8]. However, some non-oxide chalcogenide-based $p$-type transparent conductors such as Zn doped $CuAlS_2$ [17] and undoped $\alpha$-$BaCu_2S_2$ [18] show transmittance $> 80\%$ and higher hole mobility with appreciable conductivity of $\approx$ 64 S cm$^{-1}$ and 17 S cm$^{-1}$ respectively.

Recently, the Cu-Zn-S materials system has shown promise for obtaining $p$-type transparent conductors with improved conductivity. Kudo *et al.* [19] reported $(Cu_2S)_x(ZnS)_{(1-x)}$ as a $p$-type solid solution photo catalyst, however, the electrical properties were not reported. Ortiz-Ramos *et al.* also reported $p$-type transparent Cu doped ZnS thin film via chemical bath deposition (CBD) with transmittance >70% in visible range but with a sheet resistance $\approx 8.5 \times 10^4\ \Omega/\square$ [20]. Xu *et al.* used a similar CBD process to fabricate (CuS):(ZnS) nanocomposite films and attributed that the hole

conduction in these films are due to the presence of CuS phase. A conducting network of $p$-type CuS gives rise to degenerate hole conductivity in such highly conducting ($>$ 500 S cm$^{-1}$) CBD films [21]. Very recently, Chamorro *et al.* used co-sputtering from ceramic ZnS and metal Cu targets to obtain ZnS:Cu films. The films exhibited $p$-type conductivity (5 S cm$^{-1}$) with $< 40\%$ transmittance over most of the visible light range [22].

Diamond *et al.* reported that Cu alloyed ZnS deposited *via* pulsed laser deposition (PLD) at elevated temperature (550 °C) was a $p$-type transparent conductor with a maximum conductivity $\approx$ 54 S cm$^{-1}$ due to the Cu acceptor doping of the ZnS as well as the presence of minor amounts of $Cu_2S$ impurity phase [23]. With the aim of reducing the synthesis temperatures, Woods-Robinson *et al.* [9] have reported the room temperature synthesis of CuZnS films with similar values of conductivity. They also found evidence for Cu substitution into the ZnS lattice resulting in the formation of acceptor levels responsible for the degenerate hole conductivity. However, PLD as a physical vapor deposition (PVD) technique, cannot be used for large area deposition and is not really effective for fabricating films on substrates that have no epitaxial relationship with the growing film.

In the past, the PVD technique of choice for transparent conductor development has been reactive and non-reactive DC/RF sputtering due to the ease of transfer to a large area deposition process [2]. In this study, RF sputtered Cu alloyed ZnS with varying Cu content were examined. The films were characterized for their structural, morphological, optical and electrical properties. The Cu alloyed ZnS films developed in this study exhibit transmittance $\geq 75$ % in the most part of visible light range coupled with excellent hole conductivity ($\approx$ 752 S cm$^{-1}$) at room temperature. To qualitatively evaluate and compare the performance of transparent conductors, the figure of merit (FoM, $\Phi_H$) is a very important parameter. The $\Phi_H$ was calculated using the following equation proposed by Haacke [24].

$$\Phi_H = \frac{T^{10}}{R_{sh}}$$

where $R_{sh}$ is the sheet resistance and T is the transmittance. According to this procedure the FoM is calculated using the sheet resistance and the optical transmission of the transparent conductor near the maximum in the solar spectrum ($\approx$ 550 nm). We have calculated FoM of most of the well known *p*-type transparent conductors and compared with the FoM of the Cu alloyed ZnS film obtained in this work.

## 2. Experimental section

### *2.1. Experimental procedure*

$Cu_xZn_{1-x}S$ (x = 0.1, 0.2, 0.3, 0.4 and 0.5) targets of 25.4 mm diameter were made using cold isostatic press process from ZnS (anhydrous powder 99.99% trace metal basis), $Cu_2S$ (anhydrous powder 99.99% trace metal basis), and S (powder). The substrates (glass) were cleaned with methanol for five minutes and then rinsed with DI water for one minute before drying with $N_2$ gas. The substrates were immediately loaded in the load-lock chamber after drying. The deposition chamber was pumped down to the base pressure of $\approx 4 \times 10^{-8}$ torr before starting the deposition. Pre-sputtering for 15 min was done in argon atmosphere (flow rate: 2 sccm) at working pressure of 7.3 $\times 10^{-3}$ Torr with 50 W power. The Cu alloyed ZnS films were deposited on glass substrates at 350 °C *via* RF sputtering (SVT Associates SMART system) at a constant pressure of 7.3 $\times 10^{-3}$ Torr with 50 W power.

The sputtered Cu alloyed ZnS films with varying Cu content will be mentioned as F1(10 % Cu), F2 (20 % Cu) , F3 (30 % Cu), F4 (40 % Cu), and F5 (50 % Cu)

### *2.2. Characterization*

Scanning electron microscopy (Zeiss Ultra 55 FE-SEM) was used for imaging and measuring thickness of the deposited films. Structural properties of the films were obtained using X-ray diffraction (Rigaku SmartLab X- ray diffractometer equipped with Cu-K$\alpha$ source) in $\theta$-scan mode. The optical transmission and reflection of the

films were obtained at room temperature by a UV-Vis-NIR spectrometer (Lambda 950 UV-Vis spectrometer from PerkinElmer) equipped with an integrating sphere detector. Electrical properties of the films deposited on the glass substrate were analyzed by variable temperature AC Hall-effect measurement (LakeShore Model 8404 AC/DC HMS) using a van der Pauw configuration. Transmission electron microscopy (PHILIPS CM 200) with operating voltages from 20-200 kV was used to identify the ZnS and $Cu_2S$ crystal structures. Roughness of the films were measured using Atomic Force Microscopy (Bruker Nano DI3100).

## 3. Results and discussions

### *3.1. Structural analysis*

The structural characteristics of the Cu alloyed ZnS thin films grown at 350 °C on glass substrates *via* RF sputtering were investigated by XRD and SEM. Fig. 1 shows the XRD pattern of the Cu alloyed ZnS thin films. All of the films with varying Cu content, generally, showed features corresponding to the ZnS sphalerite structure with diffraction peaks at 28.6°, 33.1°, 47.6°, 56.5°, 59.1°, and 69.4° corresponding to (111), (200), (220), (311), (222) and (400) planes, respectively (JCPDS card no. 05-0566). In addition, the ratio of $I_{\{hkl\}}/I_{\{111\}}$ for the various $\{hkl\}$ peaks seen in the polycrystalline XRD pattern (Table S1) shows that these values are much smaller for (220), (311) and (400) planes. Hence, we can conclude that the films are primarily oriented along (111) and (200) planes than the corresponding values for a truly polycrystalline film.

Also, no shifts in the peak position were observed with an increase in the Cu concentration as $Cu^+$ and $Zn^{2+}$ have similar ionic radii of $\approx$ 74 pm [25]; the Cu substitution on the Zn sublattice of ZnS does not distort the crystal structure [9, 22]. However, a slight reduction in peak intensity is observed for the (111) plane with increasing Cu concentration. Concomitant with this decreasing peak intensity of the ZnS phase, an additional peak at $2\theta = 46.4°$, corresponding to (220) plane of $Cu_2S$ is

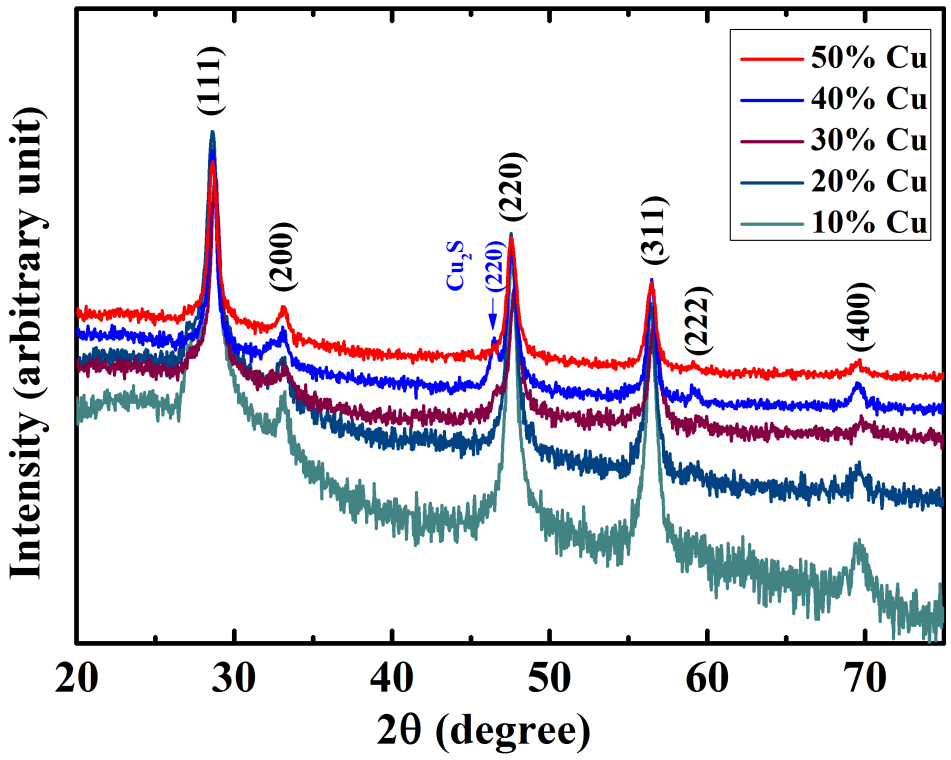


**Figure 1.** Log scale XRD patterns of Cu alloyed ZnS films with different Cu concentrations. X-ray diffraction patterns indicate the presence of sphalerite crystal phase for all Cu alloyed ZnS thin films. Planes (111), (200), (220), (311), (222) and (400) corresponding to sphelerite phase ZnS and plane (220) corresponding to $Cu_2S$ are shown. The $Cu_2S$ phase is present only in F3 and F4.

observed in those XRD patterns. At lower concentration of Cu, the peak corresponding to the $Cu_2S$ phase is not visible, but as we increase the amount of Cu ($> 20\%$) in the film, the $Cu_2S$ peak starts to appear. Interestingly, F5 does not show a sharp peak corresponding to the $Cu_2S$ phase. This could be because the $Cu_2S$ phase at this Cu concentration is in the amorphous state. Fig. S1 shows the Raman data for the Cu alloyed ZnS films. The peak at $\approx 472$ cm$^{-1}$ in the Raman spectra in Fig. S1 corresponds to the $Cu_2S$. The Raman spectra for F4 has a sharp peak at $\approx 472$ cm$^{-1}$ corresponding to the $Cu_2S$ phase. However, the peak at the same position in the Raman spectrum for F5 is broadened, corroborating our inferences from the XRD data on the same films.

The SAED pattern of F4 (Fig. 2(a)) is composed of series of rings with some bright spots which imply that the film is polycrystalline, albeit with some preferential

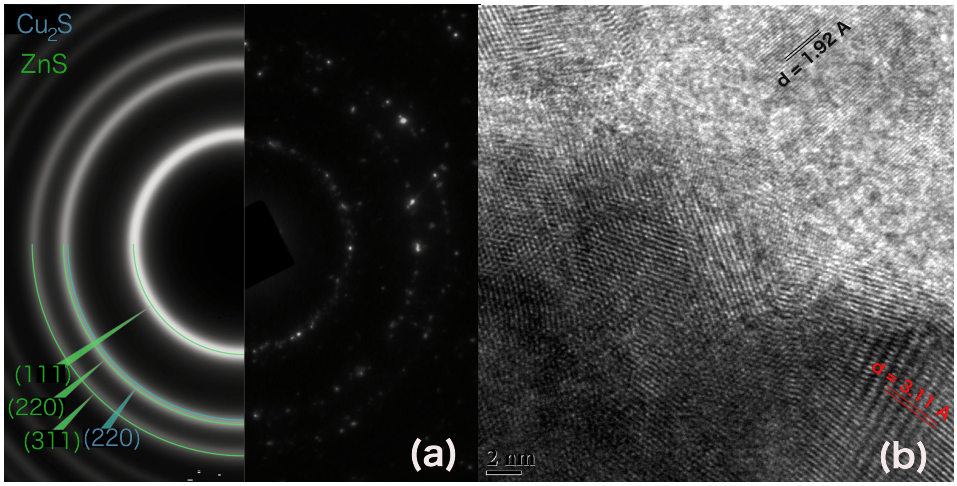


**Figure 2.** (a) Electron diffraction pattern of F4, (b) Planes (111), (220), (311) corresponding to sphelerite phase ZnS and plane (220) corresponding to $Cu_2S$ are shown.

orientation. The SAED pattern was analyzed with Diffraction Ring Profiler, which was developed for phase identification in complex microstructures [26]. It is seen that all the rings match well with the (111), (200), (220), and (311) plane of sphalerite ZnS and one diffraction ring (marked with the blue callout in the simulated pattern) could also correspond to the (220) plane of $Cu_2S$. The HRTEM image (Fig. 2(b)) clearly shows the regions with interference fringes arising from crystalline phases in that region. In the specific HRTEM image shown in Fig. 2(b), the $d$-spacing values of 1.92 Å and 3.11 Å marked for two of the crystalline regions, matches well with the $d$-spacing values for the (220) and (111) planes of sphalerite ZnS. We can also observe from HRTEM that the chosen particles are a set of nano-particles with different orientations. Again, from HRTEM, it is very difficult to distinguish between $d$–spacing values of ZnS and $Cu_2S$ for the (220) planes because the distance between the (220) planes for ZnS and $Cu_2S$ are very close $\approx$ 1.92 Å and $\approx$ 1.96 Å respectively.

### *3.2. Optical analysis*

The transmission and reflection spectrum in the wavelength range of 300 nm to 1100 nm of F1-F5 recorded with a UV-Vis spectrometer is shown in Fig. 3. All the Cu alloyed

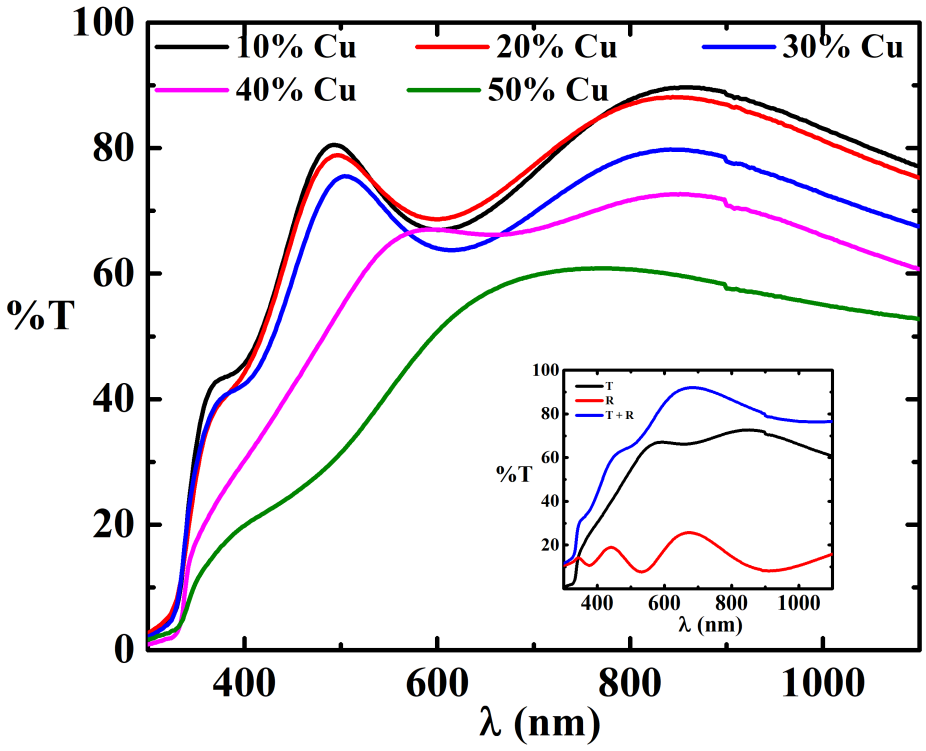


**Figure 3.** Transmission spectra of Cu alloyed ZnS films (thickness ≈ 200 nm) deposited at 350 °C. Transmission > 60% for most part of visible light range was observed for all the films except F5. Inset shows that transmission (%$T$), reflection (%$R$) and $T$+$R$ (%) spectra of F4.

ZnS films except for F5, show transmittance >60% in visible and near infrared region ($h\nu \leq 2.25$ eV). The average transmittance of the films decreases with the increasing Cu content and can be attributed to the increase in the amount of the $Cu_2S$ phase with the concomitant increase in the free carrier concentration. Fig. S3 in the supplementary information shows the plot of reflectance(%$R$) *vs* wavelength (nm). We can observe from the plot that the reflectivity in all the films are between 10% to 30 %.

The data shown in the inset of Fig. 3 is a plot of the transmission $T$, reflection $R$ and transmission + reflection ($T$+$R$) data of F4. High reflectivity in the films leads to the lower transmittance values in the UV-Vis measurement. However, the use of these films as a transparent conductor in PV applications would also include an appropriate anti-reflection coating. In that case, the intensity of light lost *via* reflection will be reduced.

Therefore, reflection-corrected transmittance is a better measure of the material quality; our best film (F4) shows transmission $> 75\%$ for the most part of the visible light range. Absorption in the films could have been due to the presence of $Cu_2S$, which possesses a band gap of $< 2.5$ eV.

### *3.3. Electrical properties*

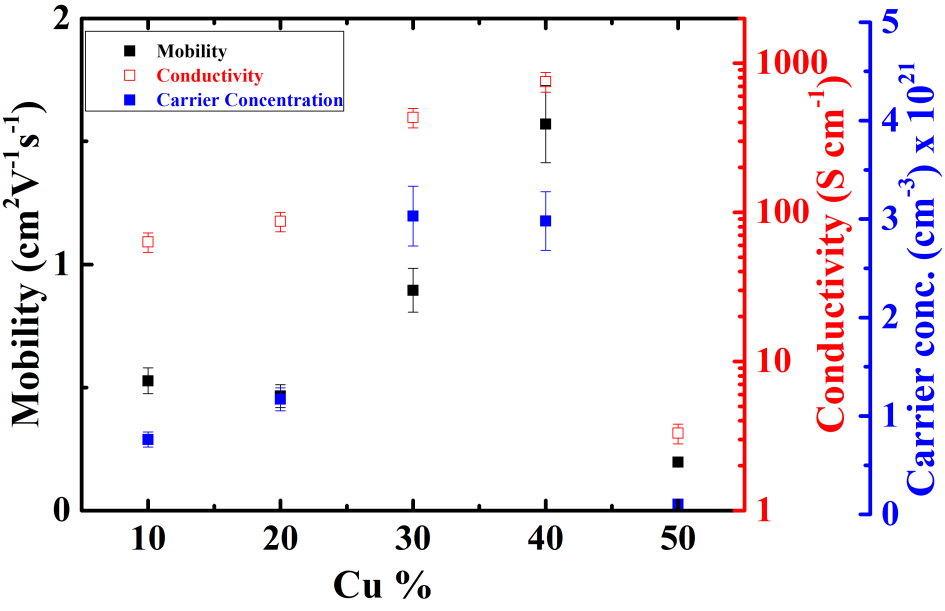


**Figure 4.** Room temperature conductivity, mobility and carrier concentration of F1-F5. There is no significant change in the condutivity as Cu content changes from 10% to 20%. Highest conductivity of $\approx 752$ S cm$^{-1}$ is obtained for F4. Conductivity of the film decreases rapidly for F5.

Fig. 4 shows the conductivity, mobility and carrier concentration of F1-F5. All the conducting films exhibited a positive Hall coefficent, indicating $p$–type material. The Hall mobility of the films varies from $\approx 0.5$ to 1.6 cm$^2$ V$^{-1}$ s$^{-1}$. Low mobility of these materials are due to the high effective mass of holes. This was also corroborated *via* Seebeck coefficient measurements; representative data for the F4 with S = +35.5 $\mu$V K$^{-1}$, is shown in Fig. 5.

Chamorro *et al.* also observed that for Cu $> 10\%$ content in RF sputtered Cu:ZnS, the film shows $p$-type conductivity [22]. From Fig. 4, it can be seen that the conductivity

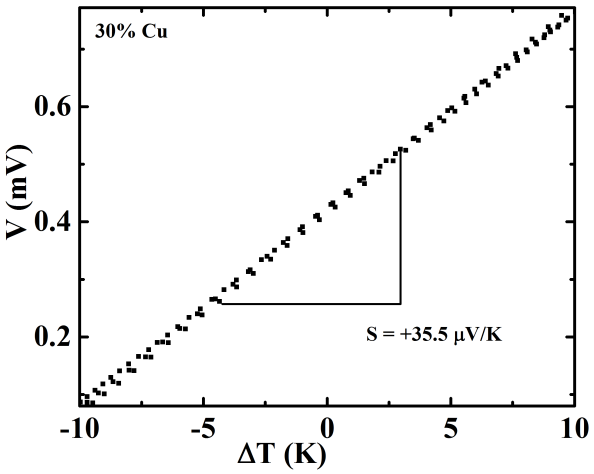


**Figure 5.** Seebeck effect measured at room temperature for F4, deposited at 350 °C. Seebeck coefficient ( $+35.5\ \mu\mathrm{V\,K^{-1}}$) confirms the $p$-type conductivity in the film.

of the films increases with increasing Cu content. Significant change in the conductivity was observed as the Cu content changes from 20% to 30% and at 40% Cu, the maximum conductivity $\approx$ 752 S-cm$^{-1}$ was observed. $p$-type conductivity in the films can be explained by the substitution of $Zn^{2+}$ by $Cu^{+}$ (substitution by $Cu^{2+}$ will not change the ionic behavior of the material) as well as the presence of $Cu_2S$. It is evident from the formation enthalpy of CuS(–53.1 kJ mol$^{-1}$) and $Cu_2S$ (–79.0 kJ mol$^{-1}$) that the $Cu^{+}$-$S^{2-}$ bond is more stable than the $Cu^{+2}$-$S^{2-}$. This also explains the presence of copper in $Cu^{+}$ ionic state [22].

Thus, the high carrier concentrations (shown as the secondary axis in Fig. 4), of the order of $10^{21}$ cm$^{-3}$ observed in these films can be attributed to the presence of crystalline $Cu_2S$ phase, which is known to have a high carrier concentration at room temperature [27]. Importantly, the decrease in the conductivity *via* the decrease in the carrier concentration as we go from 40% to 50% Cu content in the film is suggestive of the hypothesis that the presence of crystalline $Cu_2S$ phase is critical in determining the electrical transport properties of this material. So, the conductivity in films having Cu $\leq$ 20% is due to the $Cu'_{Zn}$ acceptor defects that are compensated by holes in the valence band as well as the presence of minor amount of $Cu_2S$ phase. Pham *et al.* also showed from density of state (DOS) calculation that the $Cu'_{Zn}$ contributes only to

valence band edge instead of inducing any shallow defect state [28]. Due to this, even at low temperatures all the states are ionized and gives rise to conductivity. However, with the increase of Cu content beyond 20%, excess formation of crystalline $Cu_2S$ is the major contributor to the high conductivity in these films.

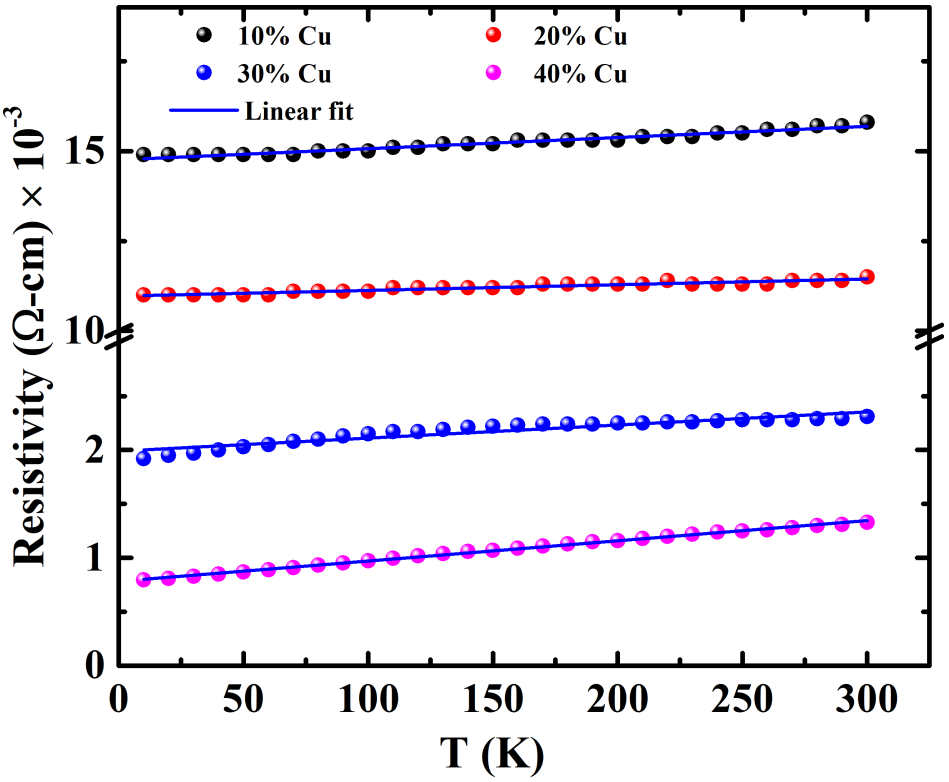


**Figure 6.** Linear fitting of the resistivity curves of F1-F4. Films are showing metallic behavior due to the presence of crystalline $Cu_2S$.

Low temperature resistivity measurements in the range of 10−300 K were conducted to study the electrical properties of the Cu alloyed ZnS films. Fig. 6 shows the resistivity *vs* temperature ($\rho$ *vs* T) plots of the films, F1−F4, where the resistivity of the films increases linearly with temperature. The linear dependence of resistivity on temperature is a typical characteristic of metals attributable to the phonon scattering in metals. The temperature coefficient of resistivity ($\alpha$) ($d\rho/dT>0$) shows a positive value for the F1−F4 in the entire range of temperature, from 10−300 K. The $\alpha$ for the most conducting film (F4) is $\approx 0.0012$ $K^{-1}$, which is comparable to that of metals. Metal like conductivity in these films can be due to the shifting of Fermi level into the valence

band as well as the presence of crystalline $Cu_2S$ in the films [28]. Crystalline $Cu_2S$ in F3 and F4 gives rise to high conductivity in the film, whereas the degenerate doping and minority $Cu_2S$ phase play important role for hole conduction in F1 and F2.

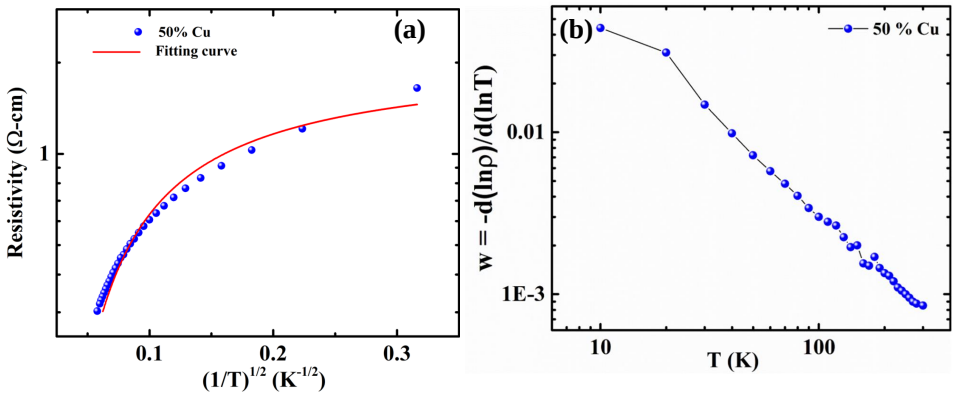


**Figure 7.** (a)Conduction in the film with 50% Cu (F5) is only due to the hopping transport mechanism. (b) Reduced activation energy as a function of T (K) for 50% Cu film.

Fig. 7(a) presents the $\rho$ *vs* $T^{-0.5}$ plot for F5. In contrast to the $\rho$ *vs* T behavior in F1-F4, F5 shows strong temperature dependence of resistivity (Fig. S4), which can be explained *via* hopping transport mechanism. The $\rho$ *vs* T data was further fitted using the equation $\rho(T) = \rho_0 exp(T_0/T)^{1/2}$, and the fit is shown as the red curve in Fig. 7(a). It can be observed that there is a good fit of the experimental plot with the hopping transport mechanism. F5 is comprised of amorphous $Cu_2S$ and Cu doped ZnS phases (Fig. 1 and Fig. S1, supporting information). Amorphous $Cu_2S$ with Cu doped ZnS together in a system can be stated as an inhomogeneous disordered granular system. In this situation, the carriers need to overcome an electrostatic barrier to hop onto a neighboring grain as probability of tunneling from grain to grain is very less [29]. Also, resistivity curve does not shows any Arrhenius type activation behavior and is well explained using hopping transport equation. The reduced activation energy, W $= -\mathrm{d}(\ln\rho)/\mathrm{d}(\ln T)$ as a function of temperature is also plotted for investigating the conducting behavior of the film as shown in Fig. 7(b) [30]. The $W < 0$ along with the

observed $d\rho/dT < 0$ also confirm the insulating nature of F5.

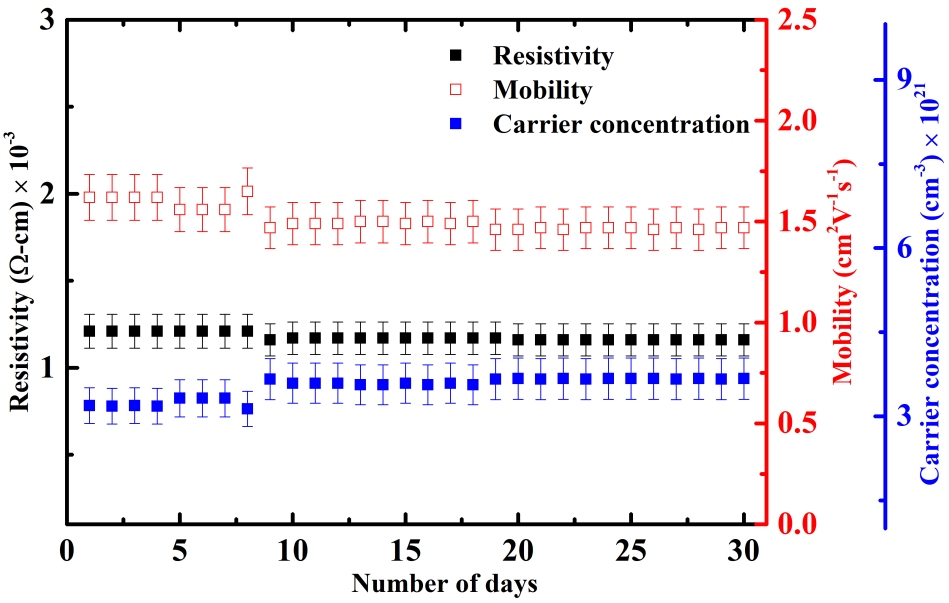


**Figure 8.** Stability test of most conducting F4 *vs* time. Film was exposed to the ambient for 30 days with resistivity measurements taken at one day intervals.

Stability studies under ambient conditions were performed for F4. Fig. 8 shows the resistivity, mobility and carrier concentration ($\rho$, $\mu$ and $p$) of this film over one month in one day intervals. Stability of transparent conductor greatly depends on thickness of the films and it is reported earlier that films with thickness 200 nm or greater are more stable [31]. We have performed stability test on 200 nm thick F4 film. Storage under ambient conditions shows excellent electrical stability and did not show any significant change in $\rho$, $\mu$ or $p$ of F4. The measured $\rho$ is $\approx 10^{-3}$ $\Omega$ cm, $\mu$ is $\approx 1.6$ cm$^2$ V$^{-1}$ s$^{-1}$ and $p$ is to the order of $\approx 10^{21}$ cm$^{-3}$ with minor variation for the total 30 days of measurement.

### *3.4. Figure of merit*

For calculating the figure of merit of our most conducting film (F4), the average of the transmittance values between 1.5 eV to 2.5 eV was considered which is $\approx 67\%$ and the sheet resistance is $\approx 66.5$ $\Omega/\square$, resulting in a FoM of 276 $\mu$S. We also used another method for calculating FoM using the transmittance at 550 nm wavelength. This method was

**Table 1.** Figure of Merit of selected $p$–type transparent conductors

| Material | $\phi_H$ ($\mu$S) | Deposition method |
|---|---|---|
| $CuAlO_2$ | 0.005 | Laser ablation [7] |
| $SrCu_2O_2$ | 0.008 | PLD [10] |
| Cu-alloyed ZnS | 7.08 | PLD [23] |
| Cu-alloyed ZnS | 1.25 | PLD [9] |
| $(Cu_2S)_x(ZnS)_{(1-x)}$ | 91.1 | CBD [21] |
| Cu-doped ZnS | 0.163 | CBD [20] |
| $CuCrO_2$ | 0.274 | Spray Pyrolysis [32] |
| $CuAlS_2$ | 68.1 | SPS [17] |
| Sr doped $LaCrO_3$ | 0.05 | MBE [33] |
| I-doped CuI | 76.2 | Sputtering [34] |
| LaCuOS | 0.028 | RF sputtering [15] |
| $CuScO_{2+x}$ | 0.001 | Sputtering [13] |
| $BaCu_2S_2$ | 6.13 | RF sputtering [18] |
| Cu alloyed ZnS | 202.5 | RF sputtering$^{This\ work}$ |

also used to calculate FoM of our best performing film as well as some of the best known $p$-type transparent conductors till date. Table 1 compares the FoM of typical $p$-type transparent conductors fabricated *via* different techniques such as PLD, CBD, RF sputtering *etc.*. FoM values shown in Table 1 were calculated using transmittance at 550 nm. To the best of our knowledge, this is the highest figure of merit obtained amongst the films deposited *via* RF sputtering technique.

## 4. Conclusion

In summary, we have fabricated $p$-type Cu alloyed ZnS thin films with hole conductivity as high as $\approx$ 752 S cm$^{-1}$ *via* RF sputtering technique. Cu alloyed ZnS with 40% Cu,

deposited at 350 °C showed the maximum conductivity and is fairly transparent in visible light range. Most conducting film showed the metallic behavior due to presence of crystalline $Cu_2S$ in the film, which can be correlated to the fact that it has high carrier concentration ($> 10^{21}$ cm$^{-3}$) at room temperature. Degenerate hole conductivity was observed in films having lower Cu concentration. TEM and XRD confirmed that all deposited films were in sphalerite structure with (111) and (220) as the primary orientations. The line and area mapping of the Cu alloyed ZnS with 40% Cu film, revealed that Cu, Zn and S were present throughout the film. The highest figure of merit of $\approx$ 202 $\mu$S was achieved among all the RF sputtered $p$-type transparent conducting films. Our results demonstrate that the $p$-type Cu alloyed ZnS is a promising candidate as a carrier selective contact in solar cells. Also, application of this material in transparent diodes, transparent transistors and light-emitting diodes are expected in further research.

## Acknowledgements

We thank James Wu for expert technical assistance in the preparation of sputtering targets. This research is based upon work supported in part by the Solar Energy Research Institute for India and the U.S. (SERIIUS) funded jointly by the U.S. Department of Energy subcontract DE AC36-08G028308 (Office of Science, Office of Basic Energy Sciences, and Energy Efficiency and Renewable Energy, Solar Energy Technology Program, with support from the Office of International Affairs) and the Government of India subcontract IUSSTF/JCERDC-SERIIUS/2012 dated 22nd Nov. 2012. TEM analysis was done at Sophisticated Analytical Instruments Facilities (SAIF) IIT Bombay, which is supported by Department of Science and Technology (DST) India. Low temperature Hall measurement was done at IRCC, IIT Bombay. Electronic characterization was performed in the Electronic Materials Program, which is supported by the Director, Office of Science, Office of Basic Energy Sciences, Materials Sciences and Engineering Division, of the U.S. Department of Energy under Contract No. DE-

AC02-05CH11231. XRD characterization work was performed by collaboration with the Joint Center for Artificial Photosynthesis (JCAP), a DOE Energy Innovation Hub, supported through the Office of Science of the U.S. Department of Energy under Award Number DE-SC0004993. YL and XJX acknowledge fellowship support from the Chinese Scholarship Council.

## References

[1] Ginley D, Hosono H and Paine D C 2010 *Handbook of transparent conductors* (Springer Science & Business Media)

[2] Ellmer K 2012 *Nat. Photonics* **6** 809–817

[3] Fortunato E, Ginley D, Hosono H and Paine D C 2007 *MRS Bull.* **32** 242–247

[4] Delahoy A E and Guo S 2011 *Transparent conducting oxides for photovoltaics* (Wiley Online Library)

[5] Morales-Masis M, De Wolf S, Woods-Robinson R, Ager J W and Ballif C 2017 *Adv. Electron. Mater.* **3** 1600529

[6] Banerjee A and Chattopadhyay K 2005 *Prog. Cryst. Growth and Charact. of Mater.* **50** 52–105

[7] Kawazoe H, Yasukawa M, Hyodo H, Kurita M, Yanagi H and Hosono H 1997 *Nature* **389** 939–942

[8] Hautier G, Miglio A, Ceder G, Rignanese G M and Gonze X 2013 *Nat. Commun.* **4** 03292

[9] Woods-Robinson R, Cooper J K, Xu X, Schelhas L T, Pool V L, Faghaninia A, Lo C S, Toney M F, Sharp I D and Ager J W 2016 *Adv. Electron. Mater.* **2** 1500396

[10] Kudo A, Yanagi H, Hosono H and Kawazoe H 1998 *Appl. Phys. Lett.* **73** 220

[11] Ueda K, Hase T, Yanagi H, Kawazoe H, Hosono H, Ohta H, Orita M and Hirano M 2001 *J. Appl. Phys.* **89** 1790–1793

[12] Yanagi H, Hase T, Ibuki S, Ueda K and Hosono H 2001 *Appl. Phys. Lett.* **78** 1583–1585

[13] Duan N, Sleight A, Jayaraj M and Tate J 2000 *Appl. Phys. Lett.* **77** 1325–1326

[14] Ingram B J, Harder B J, Hrabe N W, Mason T O and Poeppelmeier K R 2004 *Chem. Mater.* **16** 5623–5629

[15] Ueda K, Inoue S, Hirose S, Kawazoe H and Hosono H 2000 *Appl. Phys. Lett.* **77** 2701–2703

[16] Kamioka H, Hiramatsu H, Ohta H, Hirano M, Ueda K, Kmiya T, Hosono H and 2004 *Appl. Phys. Lett.* **84** 879–881

[17] Liu M L, Huang F Q, Chen L D, Wang Y M, Wang Y H, Li G F and Zhang Q 2007 *Appl. Phys. Lett.* **90** 072109

[18] Park S, Keszler D A, Valencia M M, Hoffman R L, Bender J P and Wager J F 2002 *Appl. Phys. Lett.* **80** 4393–4394

[19] Kudo A and Sekizawa M 1999 *Catal. Lett.* **58** 241–243

[20] Ortíz-Ramos D E, González L A and Ramirez-Bon R 2014 *Mater. Lett.* **124** 267–270

[21] Xu X, Bullock J, Schelhas L T, Stutz E Z, Fonseca J J, Hettick M, Pool V L, Tai K F, Toney M F, Fang X *et al.* 2016 *Nano Lett.* **16** 1925–1932

[22] Chamorro W, Shyju T, Boulet P, Migot S, Ghanbaja J, Miska P, Kuppusami P and Pierson J 2016 *RSC Adv.* **6** 43480–43488

[23] Diamond A M, Corbellini L, Balasubramaniam K, Chen S, Wang S, Matthews T S, Wang L W, Ramesh R and Ager J W 2012 *Phys. Status Solidi A* **209** 2101–2107

[24] Haacke G 1976 *J. Appl. Phys.* **47** 4086–4089

[25] Shannon R D 1976 *Acta Crystallogr. Sect. A* **32** 751–767

[26] Zhang L, Holt C M, Luber E J, Olsen B C, Wang H, Danaie M, Cui X, Tan X, W Lui V, Kalisvaart W P *et al.* 2011 *J. Phys. Chem. C* **115** 24381–24393

[27] Martinson A B, Riha S C, Thimsen E, Elam J W and Pellin M J 2013 *Energy Environ. Sci.* **6** 1868–1878

[28] Pham H H, Barkema G T and Wang L W 2015 *Phys. Chem. Chem. Phys.* **17** 26270–26276

[29] Beloborodov I, Lopatin A, Vinokur V and Efetov K 2007 *Rev. Mod. Phys.* **79** 469–518

[30] Khondaker S, Shlimak I, Nicholls J, Pepper M and Ritchie D 1999 *Phys. Rev. B* **59** 4580

[31] Minami T, Kuboi T, Miyata T and Ohtani Y 2008 *Phys. Status Solidi A* **205** 255–260

[32] Farrell L, Norton E, O'Dowd B, Caffrey D, Shvets I and Fleischer K 2015 *Appl. Phys. Lett.* **107** 031901

[33] Zhang K H, Du Y, Papadogianni A, Bierwagen O, Sallis S, Piper L F, Bowden M E, Shutthanandan V, Sushko P V and Chambers S A 2015 *Adv. Mater.* **27** 5191–5195

[34] Yang C, Knei$\beta$ M, Lorenz M and Grundmann M 2016 *Proc. Natl. Acad. Sci. U.S.A.* **113** 12929–12933